Front. Optoelectron. 2013, 6(2): 228–233
DOI 10.1007/s12200-013-0324-z

RESEARCH ARTICLE

Improved photovoltaic properties of Si quantum dots/SiC multilayers-based heterojunction solar cells by reducing tunneling barrier thickness

Yun-Qing CAO, Xin XU, Shu-Xin LI, Wei LI, Jun XU (✉), Kunji CHEN

School of Electronic Science and Engineering and National Laboratory of Solid State Microstructures, Nanjing University, Nanjing 210093, China

Abstract Si quantum dots (Si QDs)/SiC multilayers were fabricated by annealing hydrogenated amorphous Si/SiC stacked structures prepared in plasma enhanced chemical vapor deposition (PECVD) system. The microstructures were examined by transmission electron microscopy (TEM) and Raman spectroscopy, and results demonstrate the formation of Si QDs. Moreover, p-i-n devices containing Si QDs/SiC multilayers were fabricated, and their photovoltaic property was investigated. It was found that these devices show the good spectral response in a wide wavelength range (400–1200 nm). And it was also observed that by reducing the thickness of SiC layer from 4 to 2 nm, the external quantum efficiency was obviously enhanced and the short circuit current density (J_{sc}) was increased from 17.5 to 28.3 mA/cm^2, indicating the collection efficiency of photo-generated carriers was improved due to the reduced SiC barriers.

Keywords Si quantum dots (Si QDs), SiC multilayer, solar cells, transmission electron microscopy (TEM), Raman spectroscopy

1 Introduction

Si quantum dots (Si QDs) embedded in SiC host matrix have attracted much attention since they can be potentially applied in many kinds of devices, such as Si-based light source and next generation solar cells due to their novel physical properties compared with their bulk counterpart [1–4]. The band gap of Si QDs can be enlarged with the reducing of dot size because of quantum confinement effect, which provides an effective way to adjust the energy band structures by changing the Si QDs size so as to achieve wide spectral absorption [5–7]. Therefore, one can engineer the band structures of Si QDs in all Si-based tandem solar cells to match the broad solar spectrum, and in turn, the power conversion efficiency can be improved to circumvent the Shockley-Queisser limit.

Usually, Si QDs/SiO_2 multilayers were prepared by annealing Si-rich SiO_x films or hydrogenated amorphous Si (a-Si:H)/SiO_2 multilayers at high temperature. Room temperature photoluminescence (PL) and electroluminescence (EL) were achieved in those structures [8]. Recently, Si quantum dots/crystalline Si heterojunction solar cells have been studied toward the realization of all-Si tandem solar cells. Cho et al. fabricated Si QDs/SiO_2 stacked structures and observed the open-circuit voltage was increased proportionally with reducing the dots size [9]. More recently, the enhanced efficiency of multicrystalline Si solar cells by inkjet printing Si QDs at the solar cell surface has been reported. It was attributed to the down-shifting effect of Si QDs, which increased the external quantum efficiency in short wavelength range [10]. However, the main challenge for Si QDs multilayers used in solar cells is to get high density Si QDs as well as to get the reasonable carrier collection efficiency [4]. It is well known that the large band offset between Si and SiO_2 causes the low carrier tunneling probability, which will deteriorate the performance of device. Compared with SiO_2, amorphous silicon carbide (a-SiC) has a low band gap, which is helpful for increasing carrier tunneling probability through the barrier layers to improve the cell efficiency consequently [2,11]. To further improve the device performance, it is necessary to study the microstructures and physical properties of Si QDs-based multilayers. In our previous work, we fabricated Si QDs of different sizes embedded in a-SiC matrix by annealing Si-

Received March 12, 2013; accepted March 22, 2013

E-mail: junxu@nju.edu.cn

rich SiC films or a-Si/SiC multilayered structures [12,13]. An intense EL was achieved from the annealed samples and the EL peak energy shifted with the Si QDs size, suggesting the quantum confinement effect plays an important role in the emission process. In this work, we prepared Si QDs/SiC multilayers by thermally annealing amorphous Si/SiC stacked structures at 900°C and 1000°C. The microstructures and optical properties were studied. It was found that the Si QDs can be formed after 900°C annealing and the crystalline was increased with increasing the annealing temperature. With reducing the thickness of amorphous SiC barrier layers, the optical properties was almost unchanged while the electronic transport properties were improved. We further fabricated the prototype n-a-Si/(Si QDs/SiC) multilayers/p-Si heterojunction solar cells and observed the photovoltaic properties.

2 Experiments

The a-Si:H/SiC multilayers (MLs) with 6 periods were fabricated on quartz and p-Si substrates in plasma enhanced chemical vapor deposition (PECVD) system. The a-Si sublayer with 4 nm thickness was deposited by using pure silane (SiH_4), while 4 nm-thick a-SiC layers were deposited by using a gas mixture of SiH_4 and methane (CH_4) with the gas ratio R ($R = [CH_4]/[SiH_4]$) of 10. To investigate the influence of SiC barrier layer thickness on the device properties, we also fabricated the Si/SiC multilayers with 2 nm-thick SiC layer. During the deposition, the radio frequency power and the substrate temperature is kept at 30 W and 250°C, respectively. The post-treatment performed in N_2 atmosphere includes two steps, which is dehydrogenation at 450°C for 1 h and subsequently annealing at 900°C or 1000°C for 1 h. The structural change of the Si/SiC MLs before and after annealing was evaluated by Raman spectroscopy (Jobin Yvon Horiba HR800 spectrometer). The formation of Si QDs was determined by transmission electron microscopy (TEM) using Technai G2 operated at 200 kV. The optical absorption of the Si/SiC MLs was measured at room temperature by Shimadzu UV-3600 spectrophotometer.

To study the electronic and photovoltaic properties of present samples, we fabricated Si QDs/SiC multilayers on p-type Si wafers, followed by phosphorus-doped amorphous Si layers deposition on the multilayers to get p-i-n structures. Finally, Al electrode was evaporated on the surface and rear side of p-type Si wafers. The schematic diagram of solar cell is shown in Fig. 1. The current–voltage (I–V) curves of the cell devices were measured by using a Keithley 610C electrometer. The illuminated I–V characteristics were measured under an AM1.5 (100 mW/cm^2) illumination while the external quantum efficiency (EQE) spectra were collected by the spectral response measurement system.

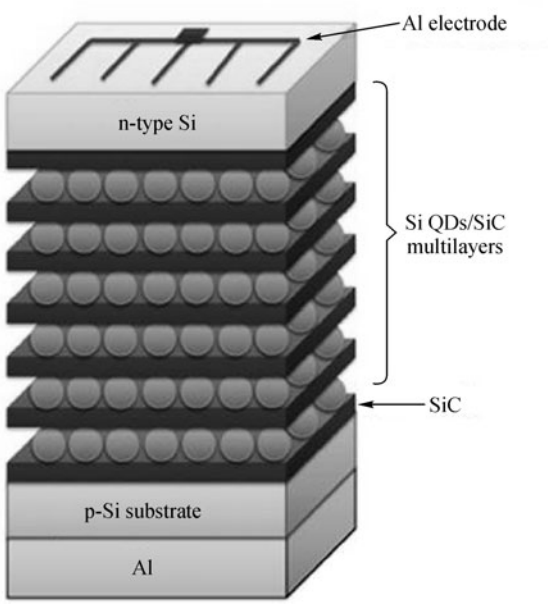

Fig. 1 Schematic diagram of solar cell containing Si QDs/SiC MLs

3 Results and discussion

Figure 2 is the cross-sectional TEM image of as-deposited a-Si (4 nm)/a-SiC (4 nm) multilayers. The layered structures and smooth interfaces of Si/SiC can be clearly identified. The thickness of a-Si and a-SiC sublayers is 4.2 and 3.9 nm, respectively, which is very close to the predesigned value (4 nm/4 nm) estimated from the deposition rule. Figures 3(a) and 3(b) show the Raman spectra of as-deposited, 900°C and 1000°C annealed multilayered samples with a-SiC layer thickness of 4 and 2 nm, respectively. Only a broad band can be found in as-deposited samples indicating their amorphous nature. After 900°C annealing, a sharp Raman band associated with crystallized Si transverse optical (TO) mode appears, which indicates that the amorphous Si layers have been crystallized to form nano crystallized Si. With increasing the annealing temperature from 900°C to 1000°C, the crystallized Raman peak becomes stronger. We fitted the Raman spectrum via the Gaussian deconvolution by three components, which is located at 480 (represents the TO mode of amorphous Si), 510 (represents the TO mode of smaller crystallized Si) and 520 cm^{-1} (represents the TO mode of larger one). The crystallinity ratio (Xc) was figured out through the formula [14]:

$$Xc = \frac{Ic}{Ic + 0.88Ia},$$

where Ic is integral area of TO mode of crystallized Si, Ia is integral area of TO mode of amorphous Si, 0.88 is Raman efficiency factor.

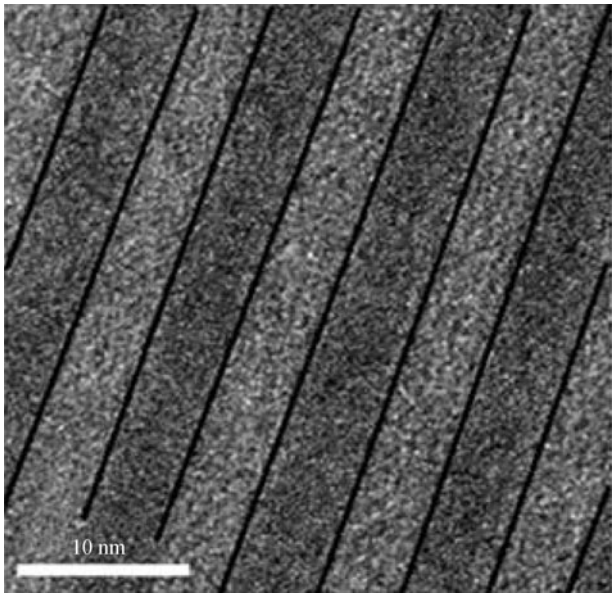

Fig. 2 TEM micrographs of as-deposited a-Si (4 nm)/a-SiC (4 nm) multilayers

It is found that *Xc* for 1000°C annealed Si/SiC MLs is higher than that for 900°C annealed ones in both Si/SiC multilayered structures, which means that higher annealing temperature promotes the crystallization process and the Si QDs with high density can be obtained. The formation of Si QDs is further identified by cross-sectional TEM observation of annealed Si/SiC multilayered samples. Figure 3(c) is the high-resolution TEM image, which exhibits the formed Si QDs after 1000°C annealing. The size of Si QDs is around 5.7 nm.

In our previous work, we found the dot size of formed Si QDs depended on the annealing temperature and the a-Si sublayer thickness. With increasing the annealing temperature, the dot size was slightly increased and the corresponding electroluminescence peak was also shifted accordingly [15,16], which is well agreement with the theoretic model based on the quantum confinement effect. Here, we also measured the optical absorption of Si QDs/SiC multilayers with various SiC thickness annealed at different temperatures. As shown in Figs. 4(a) and 4(b), the sample annealed at 1000°C exhibits the higher optical absorption coefficient than 900°C annealed ones indicates that the absorption can be enhanced by using forming dense Si QDs. However, it was found that optical absorption almost unchanged when reducing the thickness of SiC layers, which indicates that silicon quantum dots play an important role optical absorption [17].

To study the electronic and photovoltaic properties of our samples, we measured the dark current–voltage (*I–V*) relationship and illuminated *I–V* characteristics by using p-i-n structures as shown in Fig. 1. Figure 5 shows the dark *I–V* relationship of Si QDs/SiC samples annealed at 1000°C with SiC barrier thickness of 2 and 4 nm, respectively. The results reveal that the device had good rectification characteristics. The dark current can be seen exponentially enhanced under forward bias (0~1 V), while the current remained small under reverse bias (0~– 1 V). Furthermore, the dark current of Si QDs/SiC samples with SiC barrier thickness of 2 nm is remarkably higher than that of samples with 4 nm SiC sublayers as $V > 0.3$ V. Inset in Fig. 5 is the $\ln(I/V^2) - 1/V$ plot of the *I–V* curve shown in Fig. 5. The red lines are the fit of linear dependence of $1/V$. The result shows the transport via field emission (Fowler–Nordheim tunneling) of both when *V* is above 0.6 V [18]. Since the device performance of solar cells strongly depends on the photo-generated carrier collection efficiency, in the Si QDs/SiC multilayered structures, the photo-generated electrons and holes should tunnel through the SiC barriers and then be collected by the electrodes. Therefore, the SiC barriers play an important role in carrier tunneling process.

Figure 6 is the external quantum efficiency (EQE) of p-i-n device structures containing Si QDs/SiC multilayers with various SiC layer thicknesses. It shows that the EQE of cell containing Si QDs (4 nm)/SiC (2 nm) MLs is much higher than that of containing Si QDs (4 nm)/SiC (4 nm) MLs in almost whole measurement spectra range (400–1200 nm). The short circuit current density (J_{sc}) can be calculated from EQE results [19,20]. It was found that, with reducing the SiC thickness from 4 to 2 nm, the corresponding short circuit current density (J_{sc}) is obviously enhanced from 17.5 to 28.3 mA/cm^2. It was indicated that the more photo-generated carriers (both electrons and holes) can be effectively collected by the electrodes via the tunneling process by reducing the SiC barrier thickness. Inset in Fig. 6 is the *I–V* curve of cells with various SiC barrier thickness, under the illumination of AM1.5 (100 mW/cm^2) solar spectrum. The power conversion efficiency (PCE) is about 3.73%. It is worth noting that the device structure and preparation parameter are not optimized the PCE can be further improved by controlling the cell structures such as total thickness of multilayers and improving interface conditions.

4 Conclusions

In summary, Si QDs/SiC stacked structures were fabricated by annealing a-Si:H/SiC multilayers at 1000°C. Raman spectra and TEM observation revealed that the Si QDs can be formed after annealing and the crystallinity is about 69%. We also designed the photovoltaic device based on Si QDs/SiC multilayers with various SiC sublayer thickness. Both the external quantum efficiency and power conversion efficiency is obviously enhanced by reducing the SiC barrier thickness. It suggests that the reduction of the SiC barrier thickness indeed improves the carrier tunneling efficiency through the stacked structures.

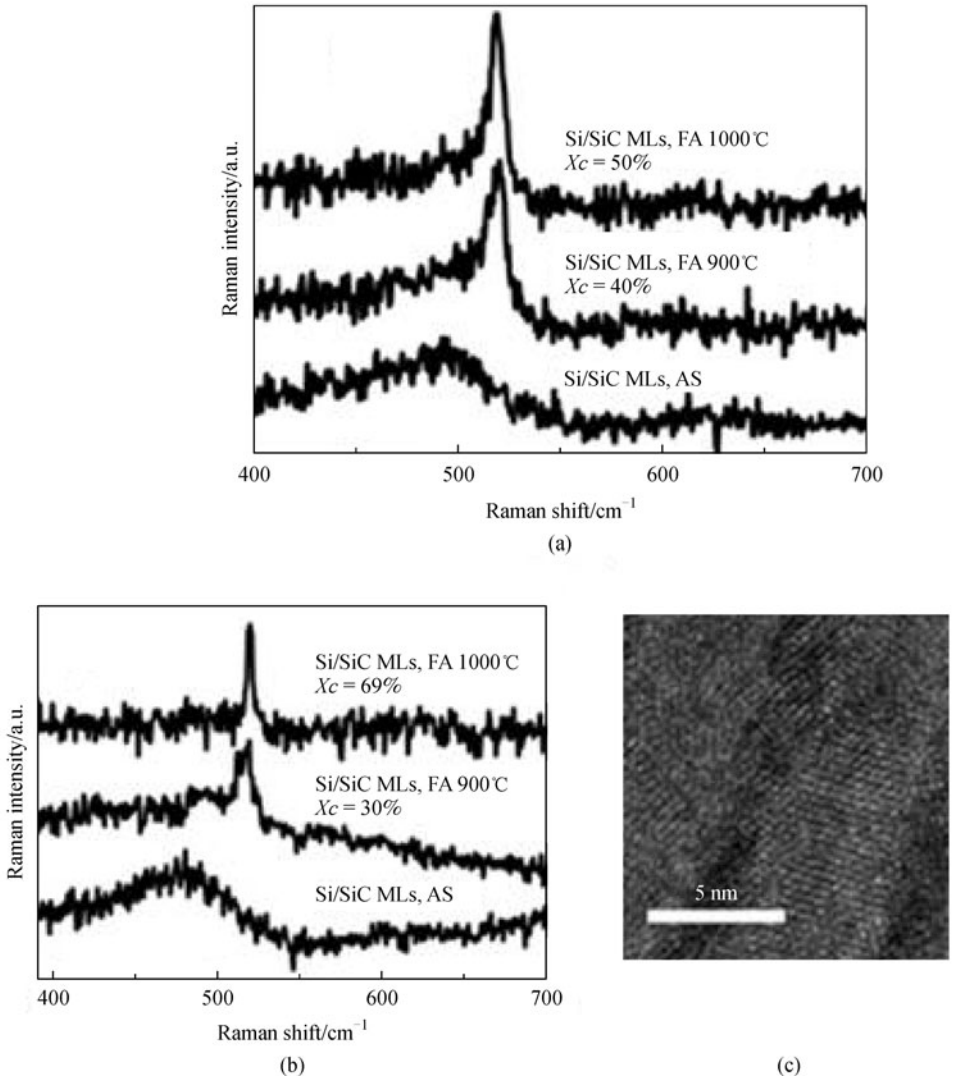

Fig. 3 Raman spectra of (a) Si (4 nm)/SiC (2 nm) MLs before and after annealing; and (b) Si (4 nm)/SiC (4 nm) MLs before and after annealing; (c) TEM micrographs of formed Si QDs after 1000°C annealing

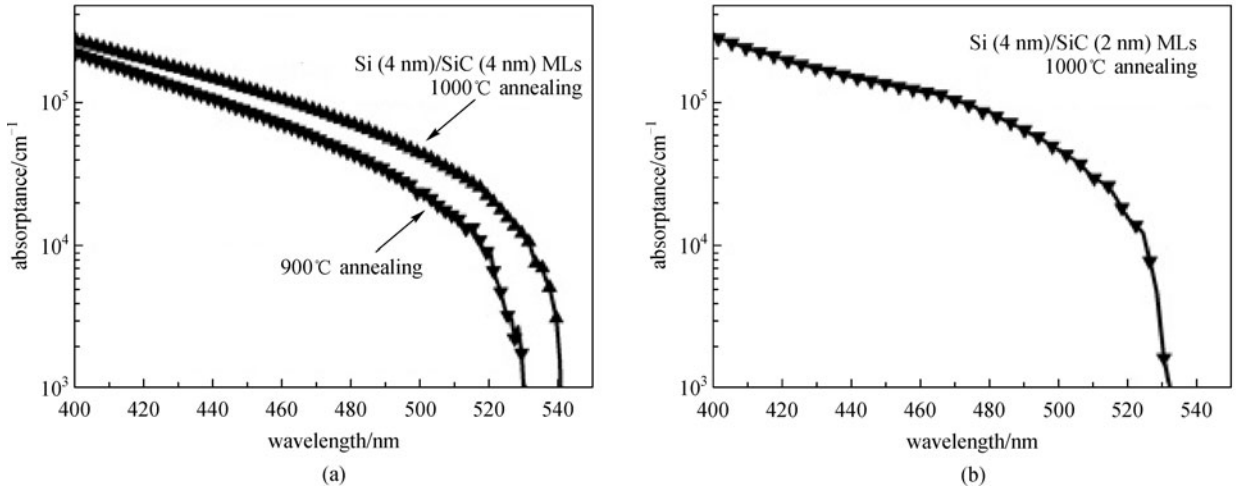

Fig. 4 Optical absorptances of (a) Si (4 nm)/SiC (4 nm) MLs after 900°C and 1000°C annealing; and (b) Si (4 nm)/SiC (2 nm) MLs after 1000°C annealing

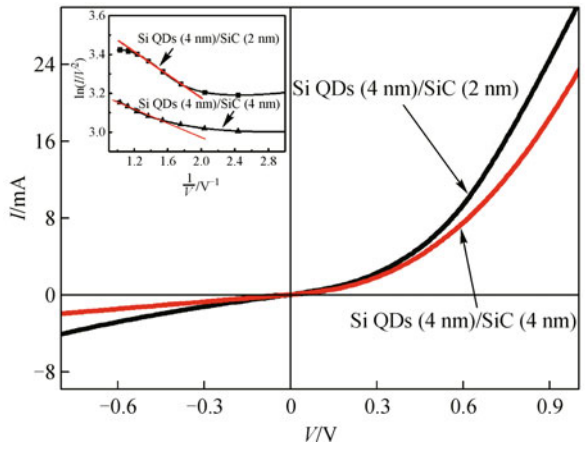

Fig. 5 Dark *I–V* characteristics of device containing 1000°C annealed Si QDs (4 nm)/SiC (4 nm) and Si QDs (4 nm)/SiC (2 nm) MLs. Inset is the ln (I/V^2)–$1/V$ plot of *I–V* curve

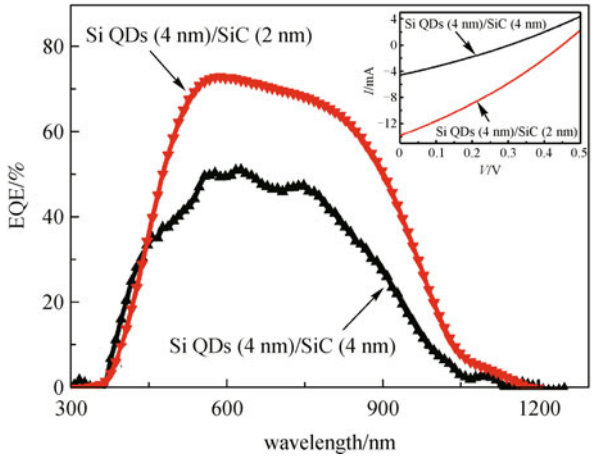

Fig. 6 External quantum efficiency of solar cells containing 1000°C annealed Si QDs (4 nm) /SiC (4 nm) and Si QDs (4 nm)/SiC (2 nm) MLs. Inset is the measured illuminated *I–V* characteristics of those samples

Acknowledgements This work was supported by the National Natural Science Foundation of China (Grant Nos. 61036001 and 11274155) and the National Major Scientific Research Program of China (No. 2013CB632101).

References

1. Surana K, Lepage H, Lebrun J M, Doisneau B, Bellet D, Vandroux L, Le Carval G, Baudrit M, Thony P, Mur P. Film-thickness-dependent conduction in ordered Si quantum dot arrays. Nanotechnology, 2012, 23(10): 105401–105410
2. Kurokawa Y, Tomita S, Miyajima S, Yamada A, Konagai M. Photoluminescence from silicon quantum dots in Si quantum dots/amorphous SiC superlattice. Japanese Journal of Applied Physics, 2007, 46(35): L833–L835
3. Baron T, Gentile P, Magnea N, Mur P. Single-electron charging effect in individual Si nanocrystals. Applied Physics Letters, 2001, 79(8): 1175–1177
4. Conibeer G, Green M A, Corkish R, Cho Y, Cho E C, Jiang C W, Fangsuwannarak T, Pink E, Huang Y D, Puzzer T, Trupke T, Richards B, Shalav A, Lind K L. Silicon nanostructures for third generation photovoltaic solar cells. Thin Solid Films, 2006, 26(511–512): 654–662
5. Perez-Wurfl I, Ma L, Lin D, Hao X, Green M A, Conibeer G. Silicon nanocrystals in an oxide matrix for thin film solar cells with 492 mV open circuit voltage. Solar Energy Materials and Solar Cells, 2012, 100: 65–68
6. Uchida G, Yamamoto K, Sato M, Kawashima Y, Nakahara K, Kamataki K, Itagaki N, Koga K, Shiratani M. Effect of nitridation of Si nanoparticles on the performance of quantum-dot sensitized solar cells. Japanese Journal of Applied Physics, 2012, 51(1): 01AD01–01AD01–5
7. Conibeer G, Green M A, König D, Perez-Wurfl I, Huang S J, Hao X J, Di D W, Shi L, Shrestha S, Puthen-Veetil B, So Y, Zhang B, Wan Z Y. Silicon quantum dot based solar cells: addressing the issues of doping, voltage and current transport. Progress in Photovoltaics: Research and Applications, 2010, 7(19): 813–824
8. Creazzo T, Redding B, Marchena E, Murakowski J, Prather D W. Tunable photoluminescence and electroluminescence of size-controlled silicon nanocrystals in nanocrystalline-Si/SiO_2 superlattices. Journal of Luminescence, 2010, 130(4): 631–636
9. Cho E C, Park S W, Hao X J, Song D Y, Conibeer G, Park S C, Green M A. Silicon quantum dot/crystalline silicon solar cells. Nanotechnology, 2008, 19(24): 245201–245205
10. Pi X D, Zhang L, Yang D R. Enhanced the efficiency of multicrystalline silicon solar cells by the inkjet printing of silicon-quantum-dot ink. Journal of Physical Chemistry C, 2012, 116(40): 21240–21243
11. Jiang C W, Green M A. Silicon quantum dot superlattices: modeling of energy bands, densities of states, and mobilities for silicon tandem solar cell applications. Journal of Applied Physics, 2006, 99(11): 114902–114908
12. Rui Y J, Li S X, Xu J, Song C, Jiang X F, Li W, Chen K J, Wang Q M, Zuo Y H. Size-dependent electroluminescence from Si quantum dots embedded in amorphous SiC matrix. Journal of Applied Physics, 2011, 110(6): 064322–064327
13. Li S X, Rui Y J, Cao Y Q, Xu J, Chen K J. Annealing effect on optical and electronic properties of silicon rich amorphous silicon-carbide films. Front. Optoelectron, 2012, 5(1): 107–111
14. Tsu R, Gonzalez - Hernandez J, ChaoS S, Lee S C, TanakaK. Critical volume fraction of crystallinity for conductivity percolation in phosphorus-doped Si:F:H alloys. Applied Physics Letters, 1982, 40(6): 534–535
15. Zhou J, Chen G R, Liu Y, Xu J, Wang T, Wan N, Ma Z Y, Li W, Song C, Chen K J. Electroluminescent devices based on amorphous SiN/Si quantum dots/amorphous SiN sandwiched structures. Optics Express, 2009, 17(1): 156–162
16. Rui Y J, Li S X, Xu J, Cao Y Q, Li W, Chen K J. Comparative study of electroluminescence from annealed amorphous SiC single layer and amorphous Si/SiC multilayers. Journal of Non-Crystalline Solids, 2012, 358(17): 2114–2117

17. Budiman M F, Hu W, Igarashi M, Tsukamoto R, Isoda T, Itoh K M, Yamashita I, Murayama A, Okada Y, Samukawa S. Control of optical bandgap energy and optical absorption coefficient by geometric parameters in sub-10 nm silicon-nanodisc array structure. Nanotechnology, 2012, 23(6): 065302–065307
18. Chiu P W, Roth S. Transition from direct tunneling to field emission in carbon nanotube intramolecular junctions. Applied Physics Letters, 2008, 92(4): 042107–3
19. Wang Q. High-efficiency hydrogenated amorphous/crystalline Si heterojunction solar cells. Philosophical Magazine, 2009, 89(28): 2587–2598
20. Taguchi M, Maruyama E, Tanaka M. Temperature dependence of amorphous/crystalline silicon heterojunction solar cells. Japanese Journal of Applied Physics, 2008, 47(2): 814–818